Applied Catalysis B: Environmental 181 (2016) 800–809

Contents lists available at ScienceDirect

Applied Catalysis B: Environmental

journal homepage: www.elsevier.com/locate/apcatb

Carbonaceous Ti-incorporated SBA-15 with enhanced activity and durability for high-quality biodiesel production: Synthesis and utilization of the P123 template as carbon source

Shih-Yuan Chen [a,*], Takehisa Mochizuki [a], Yohko Abe [a], Makoto Toba [a], Yuji Yoshimura [a], Phunthinee Somwongsa [b], Supranee Lao-ubol [b]

[a] Clean Fuel Production Group, Research Institute of Energy Frontier, Department of Energy and Environment, National Institute of Advanced Industrial Science and Technology (AIST), 1-1-1 Higashi, Tsukuba, Ibaraki 305-8565, Japan
[b] Material Innovation Department, Thailand Institute of Scientific and Technological Research (TISTR), 35 Mu 3, Khlong 5, Khlong Luang, Pathum Thani 12120, Thailand

ARTICLE INFO

Article history:
Received 11 June 2015
Received in revised form 5 August 2015
Accepted 31 August 2015
Available online 2 September 2015

Keywords:
Biodiesel fuel
Lewis solid acid catalysts
Tetrahedrally coordinated Ti species
Carbon
Coating
Long-term stability and durability

ABSTRACT

A one-pot and environmental-friendly route to synthesizing carbonaceous Ti-SBA-15 materials as weakly Lewis solid acids for transesterification of Jatropha oil with methanol to high-quality Jatropha biodiesel fuel (BDF) was successfully developed. The chemical environment and location of Ti species were controlled by the molar ratios of hydrochloride (HCl) to titanium tetraisoproproxide (TTIP) in the Ti precursors. With a HCl/TTIP molar ratio of 2.5, the tetrahedrally coordinated Ti species with weakly Lewis acid character were maximized in the superficial areas and they were associated with the catalytically active sites for transesterification. The thin carbon film, which was derived from direct carbonization of the P123 template originally existed in the channeling pores of as-made materials without adding sugar or sulfuric acid, could keep mesoporous silica framework safe from leaching during the processing steps to make Jatropha BDF. As a result, the carbonaceous Ti-SBA-15 materials gave excellent activity and durability in synthesis of high-quality Jatropha BDF, which fulfills with the specification of the international fuel standard, in both batch-type and continuous fixed-bed reaction systems. By contrast, the conventional Ti-SBA-15 materials with bare and amorphous silica framework were instable in synthesis of Jatropha BDF, in which a large amount of silica species was eluted. Although the crystalline silica framework is relatively firmed, the commercial TS-1 zeolite gave moderate activity in synthesis of Jatropha BDF, associated with the slow molecular diffusion through the micropores. The powdered or extruded TiO_2 nanoparticles with limited numbers of tetrahedrally coordinated Ti sites gave poor activities in synthesis of Jatropha BDF, and little amounts of silica and titania species from the contaminations were eluted into the Jatropha BDF.

1. Introduction

To reduce our dependence on crude oil as a limited source of energy and fuel, BDF has been widely introduced into the market of transportation sector in recent years [1]. Industrially, BDF is produced from transesterification of triglycerides (TG), the main component of vegetable oils, with methanol catalyzed by homogeneous alkali bases, such as sodium hydroxide, under mild reaction condition [2]. Since the free fatty acids (FFA) can react with alkali bases to form soap as unwanted byproduct, the vegetable oils with high acid values are pre-esterified with methanol catalyzed by homogeneous mineral acids, such as sulfuric acid, followed by several separation and purification stages before the transesterification [3]. Besides, the high-quality BDF, which fulfills with the biodiesel standard specifications, such as EN14214:2012, can be only obtained by purification of crude BDF through methanol separation, neutralization, wet washing and drying stages [4,5]. Large amounts of wastewater, organic solvents and salts are produced, which have seriously polluted our living environment. These problems can be solved by replacing of homogeneous liquid catalysts with heterogeneous solid catalysts, which are able to efficiently and durably catalyze the esterification and transesterification for high-quality BDF production [6–8].

Recent studies had demonstrated that the Ti-incorporated porous silica materials, including Ti-SBA-15, Ti-MCM-41, TS-1 and Ti-grafted SiO_2, could be used as solid acid catalysts for transfor-

* Correspondence author. Fax: +81 29 861 4532.
E-mail address: sy-chen@aist.go.jp (S.-Y. Chen).

http://dx.doi.org/10.1016/j.apcatb.2015.08.053
0926-3373/

mation of vegetable oils with methanol to BDF in the batch-type reaction system [9–13]. Among them, the Ti-SBA-15 materials with weakly Lewis acidic Ti sites gave highest activity in production of high-quality BDF, even if the common oil impurities of water or FFA were present. However, the Ti-SBA-15 materials were found to be slightly deactivated after several recycling runs in addition to a high catalyst loading of 15 wt% relative to oil required in the reaction condition [8,12,13]. Since the weakly Lewis acidic Ti species did not leach into BDF, it might be caused by leaching or harm of mesoporous silica framework during the processing steps to make BDF. So far, the industrial issue of long-term activity and durability of Ti-incorporated porous materials in production of high-quality BDF has not yet been discussed. From an industrial point of view, there is still room for development of innovative Ti-incorporated porous materials with high efficiency and durability for continuous production of high-quality BDF on a large scale. Herein, the carbonaceous Ti-SBA-15 materials with enhanced activity and durability for production of high-quality BDF in both batch-type and fixed-bed reaction systems were reported for the first time. The chemical environment and location of Ti species were found to be significantly influenced by the HCl/TTIP molar ratios in the Ti precursors. The catalyst loading relative to oil required in the batch-type reaction condition can be markedly reduced to 2 wt%, if the weakly Lewis acidic Ti species are maximized in the superficial areas. The leaching of silica can be minimized by covering of mesoporous silica framework with a thin film of carbon derived from carbonization of the P123 templates originally inside the pores. Moreover, the long-term activity and durability of carbonaceous Ti-SBA-15 materials in production of high-quality BDF were thoroughly surveyed by a continuous fixed-bed reaction system, in comparison with those of commercial TS-1 zeolite, extruded TiO_2 nanoparticles and counterpart material with bare silica framework.

2. Experimental

2.1. Synthesis of Ti-SBA-15

The Ti-SBA-15 materials were self-assembled in the weakly acidic environment using various HCl/TTIP molar ratios in the Ti precursors. In the typical synthesis, 3.0 g of P123 (Aldrich, Mn = 5800) and 2.36 g of NaCl (Wako) were thoroughly dissolved in 160 g of deionized water at 35 °C under stirring. To this solution, 8.4 g of tetraethyl orthosilicate (TEOS, TCI) was added and pre-hydrolyzed for 4 h in order to obtain the P123-silica nanocomposites. Afterward, a clearly yellowish solution obtained by mixing of TTIP (Wako) and concentrated hydrochloric acid (HCl, Wako) was stepwise added. The HCl/TTIP molar ratios were varied in the range of 1.5–10. The Ti/Si molar ratio was kept at 0.03. The gel compositions were 0.013 P123: 1 TEOS: 0.03 TTIP: 0.045–0.30HCl: 2NaCl: 220H_2O. The synthesis gels sealed in the polypropylene bottles were kept stirring at 35 °C for 20 h and then hydrothermally treated at 100 °C for another 24 h under a static condition. The as-made Ti-SBA-15 materials were obtained by filtering, washing with 300 mL of deionized water and drying at 50 °C overnight. Calcination was carried out at 500 °C for 12 h under an atmosphere of air using a ramping rate of 1 °C min^{-1}. As a result, the A500-3Ti-SBA-15 materials prepared with various HCl/TTIP molar ratios were obtained, where A represents the calcination in the air atmosphere.

2.2. Carbonization

The carbonaceous Ti-SBA-15 materials were prepared by thermal treatment of as-made Ti-SBA-15 material at 400–550 °C under an atmosphere of N_2. In all cases, the P123 templates were directly transformed into a thin film of carbon covered on the pore surfaces, where neither sugar nor sulfuric acid was used in the carbonization process. Typically, 4.0 g of as-made material prepared with a HCl/TTIP molar ratio of 2.5 was finely packed in the quartz tube and carbonized at 400–550 °C for 12 h using a ramping rate of 1 °C min^{-1} and a N_2 flow rate of 50 mL min^{-1}. The degree of P123 carbonization was surveyed by the thermogravimetric analysis (TGA) and in situ diffusion-reflectance infrared Flourier transform (DRIFT) spectroscopy. The resultant materials were designated as *Nx*-3Ti-SBA-15, where *N* and *x* represent the carbonization in the nitrogen atmosphere and the carbonization temperature with a unit of Celsius, respectively.

2.3. Characterizations

The powder X-ray diffraction (XRD) patterns were recorded in the ranges of 0.5–3° and 10–60° using a Bruker AXS DB advance diffractometer with Cu Kα radiation (λ = 1.54 Å) at 40 kV and 40 mA. The nitrogen physisorption was performed on the BELSORP-28SA instrument at 77 K. Prior to the experiment, the samples were degassed at 200 °C for 200 min under high vacuum (<10 Pa). The specific surface area (S_{BET}) was calculated by the Brunauer–Emmett–Teller (BET) method in the P/P_0 range of 0.05–0.30. The pore size distribution (PSD) curve was calculated by a modified Broekhoff-de Boer (BdB) method with the Frenkel–Halsey–Hill (FHH) equation on the nitrogen adsorption isotherms [14–16]. The pore diameter (Φ) was determined by the peak maximum of the BdB–FHH adsorption PSD curve. The total pore volume (V_{total}) was accumulated up to P/P_0 of 0.95. The specific surface area of micropores (S_{micro}) was obtained by the *t*-plot method. The TGA and differential thermal analysis (DTA) were measured by a Rigaku ThermoPlusEvo2 TG8120 instrument. Typically, the dried samples placed in the alumina holder were heated up to 800 °C with a ramping rate of 10 °C min^{-1} in air. The elemental analysis in bulk was measured by the inductively coupled plasma-optic emission spectrometer (ICP-OES) using a Thermo Scientific iCAP 6300 ICP spectrometer. The differential heat of ammonia (NH_3) chemisorption was measured by a Tokyo Riko CSA-450G microcalorimeter at 50 °C. Before the measurement, the samples were degassed at 200 °C for 1 h under high vacuum. Diffuse-reflectance (DR) UV–vis spectra were recorded by a JASCO V-570 spectrometer using an integrating sphere detector. The elemental analysis of carbon (C), hydrogen (H) and nitrogen (N) was obtained by a LECO TruSpec CHN instrument.

2.4. Transesterification of Jatropha oil with methanol

The activity and leaching test of the prepared materials as solid acid catalysts in transesterification of Jatropha oil with methanol were examined by high pressure batch-type stainless steel reactors at 200 °C under autogenous pressure. In the typical reaction, 5.0 g of Jatropha oil, 5.0 g of anhydrous methanol (Wako) and 0.10 g of dried catalyst were sealed in the batch-type stainless steel reactor lined with glass tube (internal diameter = 1.8 cm, internal height = 30 cm and volume = 76.3 mL) and purged with N_2 for five times. To start transesterification, the batch-type stainless steel reactor was quickly inserted into the pre-heated electronic furnace and vibrated constantly with a frequency of 0.5 s^{-1}. At the specific reaction time, the batch-type stainless steel reactor was removed from the electronic furnace and quickly air-cooled to the room temperature. After the catalyst was removed through a syringe filter, the Jatropha BDF was obtained by evaporation of methanol and discarding of glycerol from the reaction mixture. According to the EN 14103 and 14105 methods, the Jatropha BDF was qualitatively analyzed by Agilent 6890N GC–MS equipped Agilent J&W HP-1 non-polar column (30 m in length, 0.25 in diameter, 1 μm

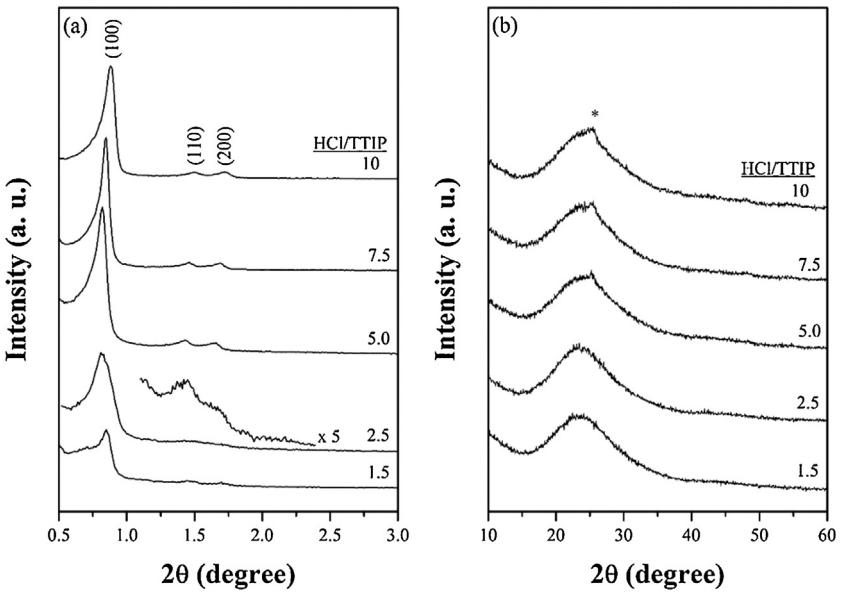

Fig. 1. (a) Small- and (b) wide-angle XRD patterns of the A500-3Ti-SBA-15 materials prepared with various HCl/TTIP molar ratios. The asterisk represents anatase titania nanoparticles.

in thickness), and quantitatively analyzed by the Agilent GC-FID instrument equipped with Agilent J&W DB-5HT (30 m in length, 0.25 mm in diameter, 1 μm in thickness) and Agilent J&W HP-1 non-polar columns [12,13].

The long-term activity and durability of the A500-3Ti-SBA-15 and N500-3Ti-SBA-15 materials prepared with a HCl/TTIP molar ratio of 2.5 in synthesis of high-quality Jatropha BDF was studied by a continuous fixed-bed reaction system at 180 °C and 0.5 MPa under an atmosphere of N_2 (30 mL min^{-1}, STP), in comparison to those of commercial TS-1 zeolite (Japan Reference Catalyst, Catalysis Society of Japan) and extruded TiO_2 nanoparticles (JGC C&C, Japan). In the typical run, the dried catalyst (1.0 g) was finely packed in the high-pressure stainless steel reactor, followed by assembling to the reaction system and in situ drying at 200 °C for 1 h under an atmosphere of N_2. To start the transesterification, the Jatropha oil and methanol were pumped into the reaction system through liquid pumps. The reaction temperature was controlled at 180 °C. The methanol-to-oil molar ratio was varied in the range of 40–120. The weight hourly space velocity (WHSV) of Jatropha oil was kept at 0.50 h^{-1}. As mentioned above, the Jatropha BDFs collected at the specific times were analyzed by the GC-FID instruments based on the procedures of the international fuel standards.

3. Results and discussion

3.1. Preparation of Ti-SBA-15 with maximum loading of active site

The A500-3Ti-SBA-15 material with maximum amount of tetrahedrally coordinated Ti(IV) species has been synthesized in the self-generated acidic environment. The pH values are tuned by varying the HCl/TTIP molar ratios in the synthesis gels. The P123 templates were completely removed from the as-made materials by calcination. In Figs. 1 and 2, the small-angle XRD patterns and N_2 adsorption–desorption isotherms show that the A500-3Ti-SBA-15 materials prepared with various HCl/TTIP molar ratios of 2.5–10 contain at least three diffraction peaks, indexed as the (1 0 0), (1 1 0) and (2 0 0) planes of 2D-hexagonal *p6 mm* pore structure, and steep hysteresis loops at P/P_0 of 0.6–0.8, associated with the well-ordered and narrowly-distributed channeling pores [17,18]. By contrast, the A500-3Ti-SBA-15 material prepared with a HCl/TTIP molar ratio of 1.5 possesses weak diffraction peaks and broad hysteresis loop. The lower the HCl/TTIP molar ratio used in the Ti precursor, the higher the pH value of the synthesis solution, which is apparently unfavorable to self-assembly of the 3Ti-SBA-15 material [19,20]. On the other hand, the wide-angle XRD patterns indicate that the 3Ti-SBA-15 materials prepared with HCl/TTIP molar ratios of 5.0–10 contain a very weak diffraction peak at $2\theta = 25.2–25.3°$, indexed as the (1 1 0) plane of anatase titania nanoparticles [21]. The formation of anatase titania nanoparticles implies that the hydrolysis and condensation rates of the Ti precursor are not in harmony with those of the P123-silica nanocomposites while the pH values of the synthesis solutions is equal to or lower than ca. 1.3.

The structural properties of the A500-3Ti-SBA-15 materials prepared with various HCl/TTIP molar ratios are tabulated in Table 1. The increases in S_{BET}, S_{Micro} and V_{total} values by increasing the HCl/TTIP molar ratios are observed whereas the trends of the Ti loading and Φ value are in reverse order. Previous studies have demonstrated that the aggregation and nature of the P123 micelles are significantly influenced by the acidity and composition of the synthesis solution [22–25]. With a relatively low pH environment, the P123 micelles are densely aggregated, where the hydrophilic PEO part is extensively inserted into the SBA-15 framework. However, the incorporation of Ti into the SBA-15 framework becomes a difficult task when the acidity of the synthesis solution is raised [20]. Consequently, the A500-3Ti-SBA-15 materials prepared with higher HCl/TTIP molar ratios have larger meso/microporous areas and volumes whereas their mesopores and Ti loadings are smaller.

The chemical environments of Ti species in the A500-3Ti-SBA-15 materials prepared with various HCl/TTIP molar ratios were examined by DR UV–vis spectroscopy (Fig. 3), in comparison to commercially available TS-1 zeolite and anatase TiO_2 powder as the reference materials. TS-1 shows a strong band centered at around 215 nm with a weak shoulder centered at 242 nm, corresponding to the ligand to metal charge transfer (LMCT) transition from O^{2-} to Ti^{4+} in the tetrahedral and octahedral coordination spheres, respectively [13,26–28]. The deconvolution of DR UV–vis spectrum shows that the relative band areas of tetrahedral and octahedral Ti species in TS-1 are 74% and 26%, respectively. In addition to two weak LMCT bands on the left shoulder, anatase TiO_2 with an average grain size of 25.5 nm shows a strong band centered at 322 nm, which is

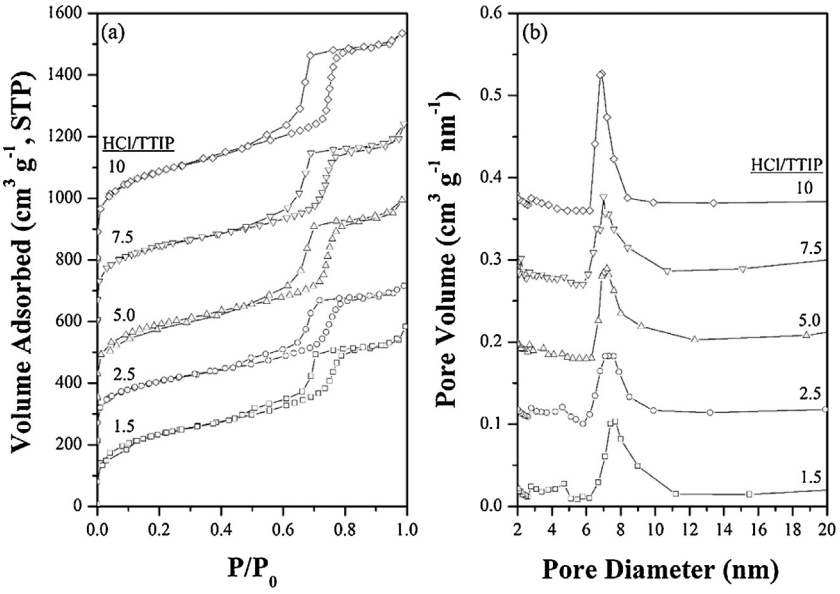

Fig. 2. (a) N_2 adsorption–desorption isotherms and (b) PSD curves of the A500-3Ti-SBA-15 materials prepared with various HCl/TTIP molar ratios. The isotherms are shifted by 0, 210, 350, 600, and 800 $cm^3\ g^{-1}$ STP, respectively. The PSD curves are shifted by 0, 0.10, 0.18, 0.27 and 0.36 $cm^3\ g^{-1}\ nm^{-1}$, respectively.

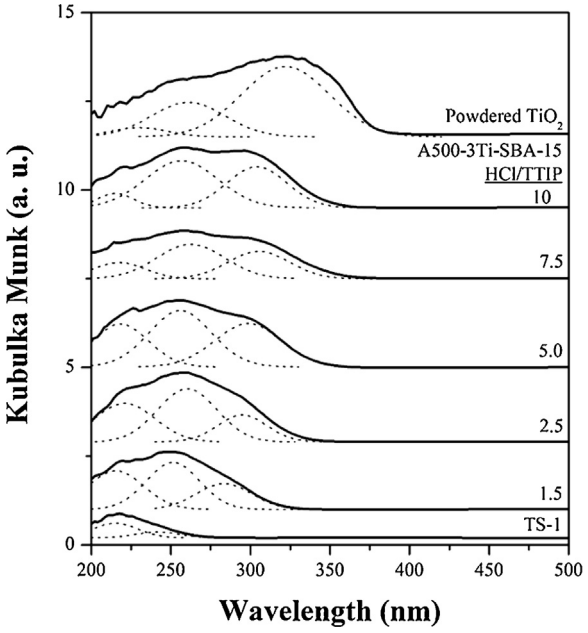

Fig. 3. DR UV–vis spectra of the A500-3Ti-SBA-15 materials prepared with various HCl/TTIP ratios, in comparison with TS-1 and powdered TiO_2 as reference materials.

associated with the electron transition from valence band to conduction band. The band gap measured from the spectrum is around 3.3 eV, consistent with the literature report [28]. For the A500-3Ti-SBA-15 materials prepared with various HCl/TTIP molar ratios, the LMCT bands from O^{2-} to Ti^{4+} in the tetrahedral and octahedral coordination spheres are observed at around 215 nm and 255 nm, respectively, and they are gradually weakened by increasing the HCl/TTIP molar ratios. Whereas, the band gap transition shifted to around 280–306 nm give an opposite trend. In combination with the results of XRD patterns and UV–vis spectra, it suggests that the A500-3Ti-SBA-15 materials prepared with HCl/TTIP molar ratios of 1.5–5 contain ultra-small TiO_2 clusters, which are X-ray amorphous and abundant in coordinately unsaturated Ti(IV) sites, such as Ti in the tetrahedral coordination sphere. Above this HCl/TTIP molar range, the X-ray visible TiO_2 nanocrystallites with relatively low amounts of coordinately unsaturated Ti(IV) sites are formed due to that the hydrolysis and condensation rates of the Ti precursor and P123-silica nanocomposites are incongruent at relatively low pH environment.

The TGA technique has been widely used to study the thermal decomposition of surfactant molecules within the porous materials, which are closely related to the superficial compositions of porous materials [17,29–31]. Fig. 4 shows the TGA and DTA profiles of as-made 3Ti-SBA-15 materials prepared with various HCl/TTIP molar ratios, in comparison with those of as-made siliceous SBA-15 material and physically mixed P123-TiO_2 compos-

Table 1
Physicochemical property and catalytic activity of the A500-3Ti-SBA-15 materials prepared with various HCl/TTIP molar ratios.[a]

HCl/TTIP (molar ratio)	pH Value[b]	S_{BET} ($m^2\ g^{-1}$)	S_{micro} ($m^3\ g^{-1}$)	V_{Total} ($cm^3\ g^{-1}$)	Φ (nm)	Ti content[c] (wt%)	Acid capacity[d] (mmol $H^+\ g^{-1}$)	FAME[e] (wt%)	G_T[e] (wt%)
1.5	1.88	651	151	0.735	7.7	4.76	1.37	72.7	5.3
2.5	1.71	759	165	0.917	7.3	3.31	2.05	81.7	4.3
5.0	1.32	861	198	0.993	7.2	2.92	1.78	70.9	5.8
7.5	1.20	870	207	1.00	7.1	2.15	1.61	63.6	7.1
10	1.07	993	226	1.14	6.9	2.10	1.49	46.0	9.0

[a] Reaction condition: 200 °C for 1 h, 5.0 g (5.61 mmol) of Jatropha oil, 5.0 g (156 mmol) of MeOH, 0.10 g of catalyst (2 wt% of oil).
[b] Synthesis gel.
[c] Based on the ICP-OES analysis.
[d] Based on the NH_3 chemisorption.
[e] Based on the specification of EN 14,103 standard, $G_T = G + 0.255 \times MG + 0.146 \times DG + 0.103 \times TG$ where G_T, G, MG, DG and TG represent the weight percentages of total glycerol (free and bound), free glycerol, monoglycerides, diglycerides and triglycerides in the samples, respectively.

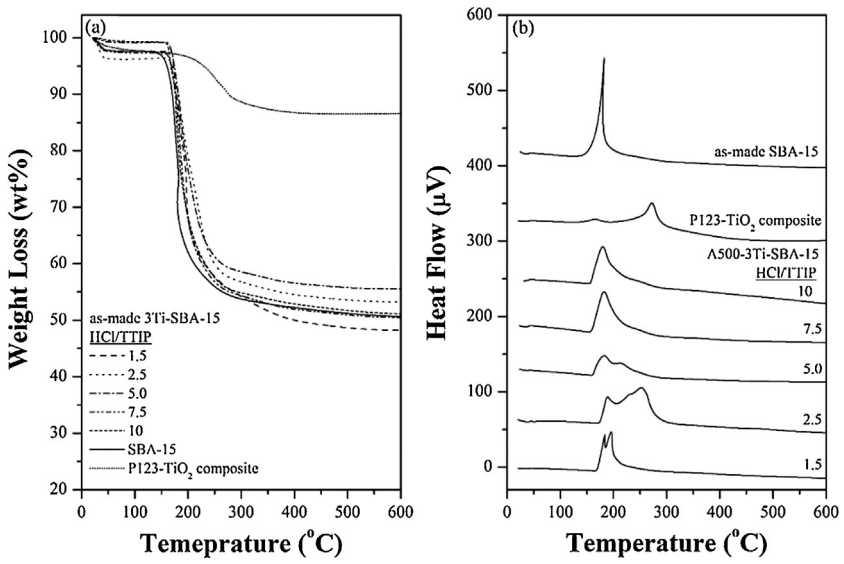

Fig. 4. (a) TGA and (b) DTA profiles of as-made 3Ti-SBA-15 materials prepared with various HCl/TTIP molar ratios, in comparison with as-made SBA-15 material and physically mixed P123-TiO_2 composite.

ite. As-made siliceous SBA-15 material was prepared in the strong acidic environment based on the recipe reported by Zhao et al. [17]. The corresponding TGA and DTA profiles show a single weight loss (46.6 wt%) with a sharp DTA peak centered at 182 °C, associated with the thermal decomposition of P123 triblock copolymer slightly embedded in siliceous pore walls [32–34]. The physically mixed P123-TiO_2 composite was obtained by fine grinding of P123 triblock copolymer (ca. 10 wt%) and anatase TiO_2 powder. The corresponding TGA and DTA profile contains a steep weight loss with a DTA peak centered at 272 °C, associated with the thermal decomposition of P123 triblock copolymer interacted with the tetrahedrally coordinated Ti sites on the TiO_2 particles through weak coordination bonds [35]. The other weak weight loss with a DTA peak centered at 164 °C should have to do with the thermal decomposition of neat P123 triblock copolymer. For the as-made 3Ti-SBA-15 materials prepared with various HCl/TTIP molar ratios, the weight losses of P123 triblock copolymer are slightly varied in the range of 43.6–49.3 wt% whereas the DTA peaks are broadened or split at around 165–300 °C. It suggests that the superficial compositions of the A500-3Ti-SBA-15 materials are significantly influenced by the HCl/TTIP molar ratios in the synthesis gels. As compared with the results of as-made SBA-15 material and physically mixed P123-TiO_2 composites, the DTA peak centered at around 180–190 °C can be assigned as the thermal decomposition of P123 triblock copolymer embedded in siliceous pores. The other DTA peak appeared at higher temperature region should have to do with the thermal decomposition of P123 triblock copolymer interacted with the tetrahedrally coordinated Ti sites on the ultra-small TiO_2 clusters or nanocrystallites. In other words, the A500-3Ti-SBA-15 material prepared with a HCl/TTIP molar ratio of 2.5 is full of tetrahedrally coordinated Ti species incorporated in the superficial pore walls. Outside this HCl/TTIP molar ratio, the gradual merging of two DTA peaks suggests that the ultra-small TiO_2 clusters or nanoparticles tend to incorporate in the inner pore walls.

The acid capacity, strength and nature of the A500-3Ti-SBA-15 materials prepared with various HCl/TTIP molar ratios were examined by NH_3 chemisorption and in situ DRIFT spectra of pyridine adsorption (Figs. 5 and 6). Fig. 5 shows that the acid capacity and strength of the A500-3Ti-SBA-15 materials are as a function of the HCl/TTIP molar ratios. Among them, the A500-3Ti-SBA-15 material prepared with a HCl/TTIP molar ratio of 2.5 shows highest acid capacity and strength, and its can be classified as weakly solid Lewis

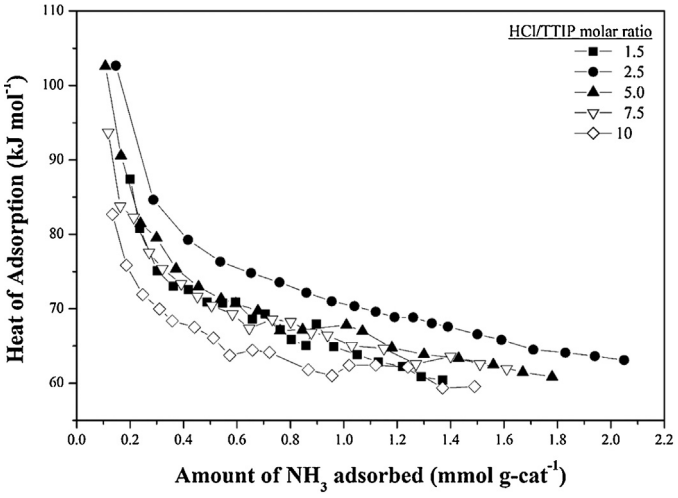

Fig. 5. Differential heat of NH_3 adsorption over the A500-3Ti-SBA-15 materials prepared with various HCl/TTIP molar ratios.

acid (also see Table 1 and Fig. 6(a)). It represents that the tetrahedrally coordinated Ti species as Lewis acid sites are maximized on the superficial area of the A500-3Ti-SBA-15 material prepared with a proper HCl/TTIP molar ratio of 2.5.

The transesterification of Jatropha oil with methanol catalyzed by the A500-3Ti-SBA-15 materials prepared with various HCl/TTIP molar ratios was conducted in a batch-type stainless steel reactor at 200 °C for 1 h. The methanol-to-oil molar ratio and the catalyst weight were kept at 28 and 2 wt%, respectively. Table 1 shows that the FAME content is increased by increasing the HCl/TTIP molar ratio from 1.5 to 2.5, and then progressively decreased as the HCl/TTIP molar ratio is further increased. It is interesting that the variation in FAME content as a function of the HCl/TTIP molar ratio is almost in the same trend as the change in acid capacity of the A500-3Ti-SBA-15 materials mostly derived from the tetrahedrally coordinated Ti species (ESI, Fig. S1). It is a fact that the catalytically active sites for transesterification of Jatropha oil with methanol into Jatropha BDF are associated with the tetrahedrally coordinated Ti species with Lewis acid property. With a proper HCl/TTIP molar ratio of 2.5, the resultant A500-3Ti-SBA-15 material with a large

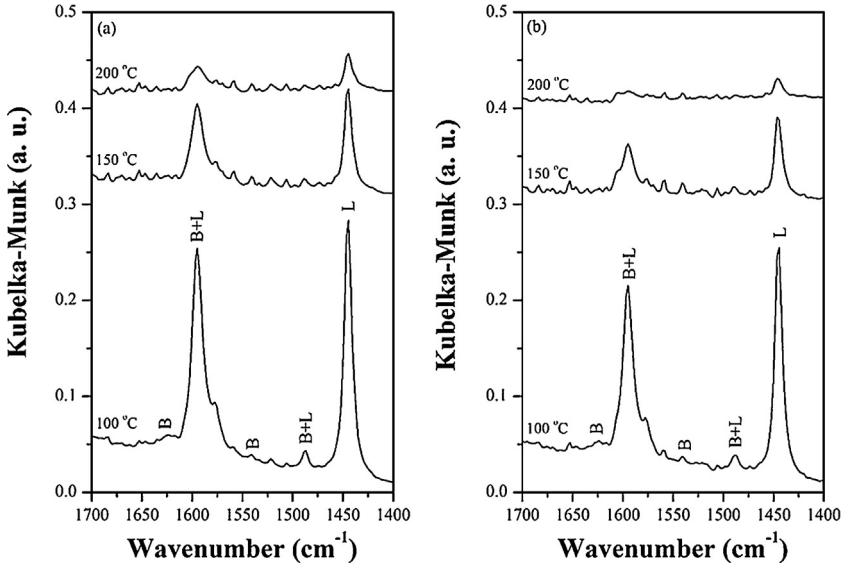

Fig. 6. In situ DRIFT spectra of pyridine adsorption on (a) A500-3Ti-SBA-15 and (b) N500-3Ti-SBA-15 materials recorded at 100–200 °C.

amount of tetrahedrally coordinated Ti species in the superficial area is efficient in catalyzing the Jatropha BDF synthesis. Above this ratio, the X-ray visible titania nanoparticles gradually formed in the counterpart materials have a negative influence on Jatropha BDF synthesis. Below this ratio, the activity of the counterpart material in Jatropha BDF synthesis is decreased due to its less accessible Ti species inside the pore walls.

According the EN14538 standard, the ICP-OES measurement can be utilized to determine the soap building elements, phospholipids and undesired contaminations in Jatropha BDF, which is synthesized by the A500-3Ti-SBA-15 material prepared with a HCl/TTIP molar ratio of 2.5. The ICP-OES data show that the soap building elements, such as Na, K, Ca and Mg, and phospholipids, in Jatropha BDF are lower than the specification of the EN14214:2012 standard (ESI, Table S1). It is clear that the formation of soap can be ignored in the reaction condition. Moreover, the influence of phosphorus on the property of catalytic converters and exhausting control system can be minimized when burning Jatropha BDF with ultra-low *P* content. About the undesired contaminations, the Ti concentration in Jatropha BDF is lower than the detection limit, indicating that the tetrahedrally coordinated Ti species as the catalytically active sites for Jatropha BDF synthesis are stable under the batch-type synthesis condition (Table 2). However, the Si concentration in Jatropha BDF is promptly increased to 76 ppm, suggesting that a small portion of mesoporous silica framework is eluted from the A500-3Ti-SBA-15 material into Jatropha BDF.

3.2. Carbonaceous Ti-SBA-15 with enhanced activity and stability

Recent reports have attempted to improve the stability of mesoporous materials by a light coating of carbon species on the surfaces [36–41]. In the conventional process, the mesoporous materials were impregnated with sugar solution, such as sucrose and glucose, and sulfuric acid, followed by carbonization at high temperature under an inert atmosphere. However, the conventional process is cost-ineffective and environmentally-unfriendly due to that the impregnation of sugar solution is a necessary step and the hazardous sulfur oxides are released during the sulfuric acid-catalyzed carbonization process. In this work, neither sugar nor sulfuric acid was used in the carbonization process. The carbonaceous 3Ti-SBA-15 materials were obtained by direct carbonization of as-made 3Ti-SBA-15 material prepared with a HCl/TTIP molar ratio of 2.5 at 400–550 °C for 12 h under an atmosphere of N_2. The P123 template as the only carbon source originally located in the pores was thermally transformed into a thin film of carbon species remained on the pore surfaces. Fig. 7 exhibits that the small-angle XRD patterns of carbonaceous 3Ti-SBA-15 materials resemble that of the A500-3Ti-SBA-15 material, indicating that the carbonization has no significant influence on the pore structure and ordering. In comparison with the A500-3Ti-SBA-15 material, the carbonaceous 3Ti-SBA-15 materials show a relatively weak diffraction band in the 2θ range of 15–40°, which is associated with the amorphous nature of mesoporous silica materials [35,42,43]. This result implies that the carbonaceous 3Ti-SBA-15 materials with relatively dense silica framework are formed. In Fig. 8, the N_2 physisorption study shows that the carbonaceous 3Ti-SBA-15 materials contain a classically type IV isotherm with a steep hysteresis H_1 loop at relatively high P/P_0 region of 0.6–0.8, corresponding to large and channeling pores. The BdB–FHH adsorption PSD curves exhibit that the Φ values are decreased in increasing the carbonization temperature, associated with the structural shrinkage by further silica condensation during carbonization. It is noteworthy that the PSD curves become narrower when the carbonization temperatures are higher than 500 °C. This phenomenon is an indication that the P123 template occupied in the channeling pores has completely transformed into a thin film of carbon species homogeneously covered on the siliceous pore surfaces.

The TGA–DTA and DRIFT techniques were utilized to survey the influence of carbonization temperature on transformation of the P123 template to a thin film of carbon species remained on the pore surfaces of carbonaceous 3Ti-SBA-15 materials. Fig. 9(a) shows that the weight loss curves of carbonaceous 3Ti-SBA-15 materials can be divided into three groups, i.e., the desorption of physically adsorbed water within 25–130 °C, the decomposition of non-carbonized P123 template within 180–350 °C and the decomposition of thin carbon film within 350–630 °C, respectively [17,34]. With the increase of carbonization temperature, the non-carbonized P123 template is gradually invisible and the decreases in physically adsorbed water and thin carbon film are observed. The DTA peak associated with the decomposition of thin carbon film shifts to high temperature region as the carbonization temperature is increased (Fig. 9(b)). The elemental analysis exhibits that the H/C molar ratios of carbonaceous 3Ti-SBA-15 materials are decreased in increasing the carbonization temperature (ESI, Table S2). The

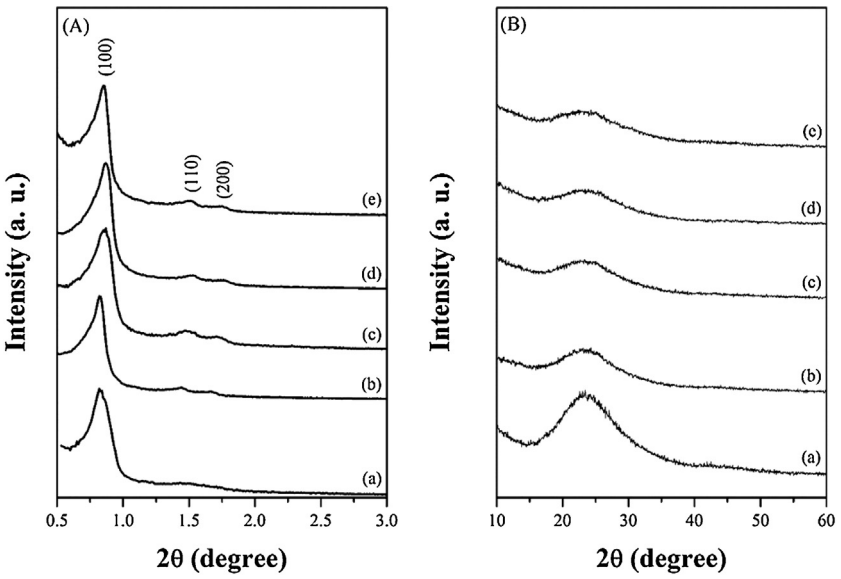

Fig. 7. (A) Small- and (B) wide-angle XRD patterns of (a) A500-3Ti-SBA-15, (b) N400-3Ti-SBA-15, (c) N450-3Ti-SBA-15, (d) N500-3Ti-SBA-15 and (e) N550-3Ti-SBA-15.

DRIFT spectra further confirm that the carbonaceous 3Ti-SBA-15 materials have nearly no characteristic bands of the C—H and C—O groups on the P123 templates and relatively weak bands of surface silanol groups (ESI, Figs. S2 and 3). It is specially noticed that the amounts of physically adsorbed water on carbonaceous 3Ti-SBA-15 materials are apparently lower than that of the A500-3Ti-SBA-15 material. Besides, for the carbonaceous 3Ti-SBA-15 materials, the weight loss owning to further condensation of mesoporous silica framework is hardly observed at high temperature region (>630 °C). It is therefore suggested that the enhanced surface hydrophobicity should have to do with the relatively dense silica framework with a light coating of carbon species. Characterizations by these conventional techniques deduce that the carbonaceous 3Ti-SBA-15 materials with relatively dense and hydrophobic carbon/silica composite framework are successfully prepared by thermal treatment of the as-made counterpart material under an inert atmosphere.

Table 2 shows the structural property and acid capacity of carbonaceous 3Ti-SBA-15 materials. All of the carbonaceous 3Ti-SBA-15 materials have higher S_{BET} and V_{Total} values than the A500-3Ti-SBA-15 material. It is another indication that a thin film of carbon derived from the P123 template is homogeneously covered on the pore surfaces of carbonaceous 3Ti-SBA-15 materials without pore blockage. Among the carbonaceous 3Ti-SBA-15 materials, the decreases in S_{BET} and V_{Total} values in increasing the carbonization temperature are consequent on the removal of thin carbon film and further silica condensation. Noted that the unit cell parameter (a_0), wall thickness (W_t) and Φ values of the N500-3Ti-SBA-15 material are slightly lower than those of the A500-3Ti-SBA-15 material. It is a fact that the density of the carbon/silica composite framework is slightly higher than that of bare silica framework, due to better silica condensation upon carbonization in an inert atmosphere. Regarding to the acidic property, the in situ DRIFT spectra of pyridine adsorption over the N500-3Ti-SBA-15 material resemble that of the A500-3Ti-SBA-15, indicating that the carbonization process has no significant influence on Lewis acid nature (Fig. 6). The decrease in spectral intensity of the N500-3Ti-SBA-15 material suggests that the tetrahedrally coordinated Ti species on the superficial areas are slightly hindered by a slight coating of carbon species. The differential heat of NH_3 adsorption study further explores the influence of carbonization temperature on acid strength and capacity of carbonaceous 3Ti-SBA-15 materials (Table 2; ESI, Fig. S4). The N500-3Ti-SBA-15 material with a proper amount of thin carbon film shows highest acidic strength and capacity. The decreases in acidic strengths and capacities of the A450-3Ti-SBA-15 and N450-3Ti-SBA-15 materials are associated with the hindrance of tetrahedrally coordinated Ti species by

Table 2
Physicochemical property and catalytic activity of the carbonaceous 3Ti-SBA-15 and reference materials.[a]

Materials	a_0 (nm)[b]	W_t (nm)[c]	S_{BET} ($m^2\,g^{-1}$)	V_{Total} ($cm^3\,g^{-1}$)	Φ (nm)	Acid capacity (mmol H^+ g-cat^{-1})	Jatropha BDF			
							FAME (wt%)	G_T (wt%)	Si (ppm)[d]	Ti (ppm)[d]
Blank	–	–	–	–	–	–	7.2	10	4.5	0
Powdered TiO_2[e]	–	–	128	0.32	9.2	0.590	23.6	9.6	7.2	0
Extruded TiO_2[e]	–	–	164	0.38	7.9	0.710	43.5	9.2	9.3	0
TS-1	–	–	405	0.27	~0.50	1.21	62.4	7.6	35	0
A500-3Ti-SBA-15	12.3	5.0	759	0.917	7.3	2.05	81.7	4.3	76	0
N400-3Ti-SBA-15	12.9	5.1	879	1.03	7.8	1.19	72.0	5.3	94	0
N450-3Ti-SBA-15	12.4	5.0	854	1.03	7.4	1.33	76.3	5.3	30	0
N500-3Ti-SBA-15	12.0	4.8	797	0.980	7.2	1.56	86.1	3.4	16	0
N550-3Ti-SBA-15	11.7	4.7	768	0.937	7.0	1.29	84.7	3.7	18	0

[a] Reaction condition: 200 °C for 1 h, 5.0 g (5.61 mmol) of Jatropha oil, 5.0 g (156 mmol) of MeOH, 0.10 g of catalyst.
[b] Unit cell parameter (a_0) = $2(d_{(100)}/\sqrt{3})$.
[c] Wall thickness (W_t) = $a_0 - \Phi$.
[d] Based on the ICP-OES analysis.
[e] Purchased from JGC C&C Co., Ltd., Japan.

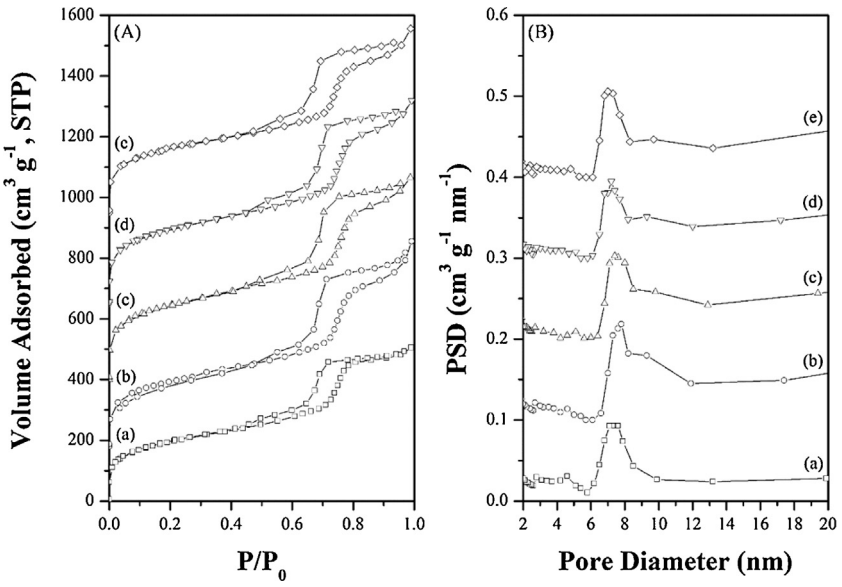

Fig. 8. (A) N_2 adsorption–desorption isotherms and (B) PSD curves of (a) A500-3Ti-SBA-15, (b) N400-3Ti-SBA-15, (c) N450-3Ti-SBA-15, (d) N500-3Ti-SBA-15 and (e) N600-3Ti-SBA-15. The isotherms are shifted by 0, 180, 400, 650, and 950 $cm^3\,g^{-1}$ STP, respectively. The PSD curves are shifted by 0, 0.10, 0.20, 0.30 and 0.40 $cm^3\,g^{-1}\,nm^{-1}$, respectively.

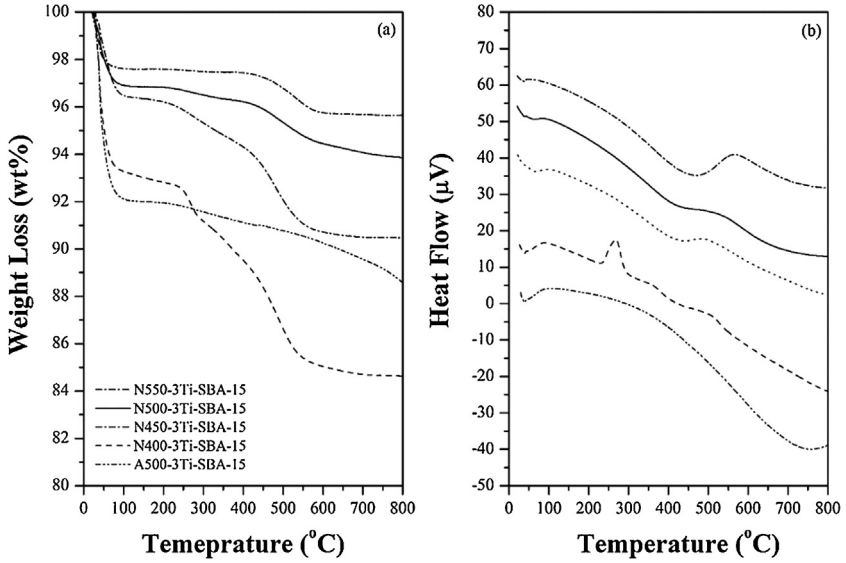

Fig. 9. (a) TGA and (b) DTA profiles of the siliceous and carbonaceous 3Ti-SBA-15 materials prepared with a HCl/TTIP ratio of 2.5.

Table 3
The composition and impurity of Jatropha BDFs synthesized by the N500-3Ti-SBA-15 and reference materials.[a]

EN14214:2012		N500-3Ti-SBA-15		A500-3Ti-SBA-15		Extruded TiO_2	TS-1
		2 h	70 h	2 h	70 h	70 h	70 h
FAME content (wt%)	min 96.5	96.9	98.2	95.9	96.4	68.9	47.3
TG (wt%)	max 0.20	0.080	0.082	0.23	0.34	25	32
DG (wt%)	max 0.20	0.056	0.19	0.72	1.3	6.4	10
MG (wt%)	max 0.70	0.48	0.36	1.90	0.74	1.4	5.4
G (wt%)	max 0.20	0.15	0.0044	0.062	0.0011	0.071	0.14
G_T (wt)	max 0.15	0.30	0.13	0.68	0.35	3.9	6.3
Si (ppm)	n.d.	3.5	1.6	133	88	2.8	12
Ti (ppm)	n.d.	0	0	0	0	9.4	0
Na + K (ppm)	5.0	0.18	0.085	4.1	0.24	0.13	0.65
Ca + Mg (ppm)	5.0	0.12	0	0.29	0.083	0.58	3.5
P (ppm)	4.0	0	0	0.54	0.15	0.17	0.91

[a] The reaction condition: 180 °C and 5 bar for 2 or 70 h, $WHSV_{oil}$ of 0.50 h^{-1}, the oil/methanol molar ratio of 100.

such large amounts of carbon films remained on the pore surfaces. By contrast, the tetrahedrally coordinated Ti species are partially buried in the silica frameworks due to further silica condensation when the carbonization temperature is equal to or higher than 550 °C [28,44].

Table 2 compares the activity of carbonaceous 3Ti-SBA-15 materials in Jatropha BDF synthesis with that of reference materials. Here, the batch-type reaction condition was as follows: 2.0 wt% of catalyst to Jatropha oil, a methanol-to-oil molar ratio of 28, a reaction temperature of 200 °C and a reaction period of 1 h. The catalytic study exhibits that the FAME content increases in the follow manner: blank < powdered or extruded TiO_2 < TS-1 < 3Ti-SBA-15 with bare or carbonaceous silica framework. Whereas, the G_T value gives an opposite trend. The N500-3Ti-SBA-15 and N550-3Ti-SBA-15 materials are superior to the A500-3Ti-SBA-15 material in catalyzing the transesterification of Jatropha oil with methanol into Jatropha BDF. It indicates that the tetrahedrally coordinated Ti species on the carbonaceous silica frameworks are accessible to the oil molecules when the carbonization temperature is equal to or higher than 500 °C. Besides, the carbonaceous framework with hydrophobic property is of great benefit to the molecular diffusion. By contrast, the decrease in FAME contents over the N400-3Ti-SBA-15 and N450-3Ti-SBA-15 materials reveals that the tetrahedrally coordinated Ti species are partially hindered by such large amounts of carbon species remained on the pore surfaces. The relatively low activity of commercial TS-1 zeolite in Jatropha BDF synthesis is attributed to the slow molecular diffusion through the micropores. The activities of powdered or extruded TiO_2 nanoparticles in Jatropha BDF synthesis are quite low, due to that the coordinative unsaturation sites are limited on the crystalline surfaces. The leaching of silica and titania from the above catalysts to the Jatropha BDFs was carefully examined by the ICP-OES technique. In all cases, the leaching of titania can be negligible, indicating that Ti is firm enough to be used as a Lewis acid site for production of Jatropha BDF in the batch-type reaction system. By contrast, the Si concentrations in Jatropha BDFs are found to be increased in the following manner: blank < powdered or extruded TiO_2 < N500-3Ti-SBA-15 ~ N550-3Ti-SBA-15 < N450-3Ti-SBA-15 < TS-1 < A500-3Ti-SBA-15 < N400-3Ti-SBA-15. For the blank test, a little leaching of silica is probably derived from the batch-type reaction system lined with glass inlet. The Si concentrations of Jatropha BDFs synthesized by the powdered or extruded TiO_2 nanoparticles are slightly increased to 7–9 ppm, probably associated with the dissolution of the contaminations. For the Ti-incorporated porous materials, the leaching of silica is mostly related with the composition and framework crystallinity. The Si concentration of Jatropha BDF synthesized by the A500-3Ti-SBA-15 material with amorphous silica framework is around 2-3 times higher than that by commercial TS-1 zeolite with crystalline silica framework. However, the Si concentrations of Jatropha BDFs synthesized by the carbonaceous Ti-SBA-15 materials are remarkably reduced, except the N400-Ti-SBA-15 material. It is clear that the leaching of mesoporus silica framework can be indeed prevented by a light coating of carbon species on pore surfaces. The Jatropha BDF synthesized by the N400-3Ti-SBA-15 material contains a high concentration of Si, probably due to that the condensation of silica and carbonization of P123 templates are incomplete at relatively low carbonization temperature.

3.3. Continuous production of high-quality BDF

The long-term activity and durability of carbonaceous N500-3Ti-SBA-15 material in continuous production of Jatropha BDF were examined by a fixed-bed reaction system at 180 °C and 0.5 MPa, in comparison with those of reference materials. In Fig. 10, the N500-3Ti-SBA-15 and A500-3Ti-SBA-15 materials with large and

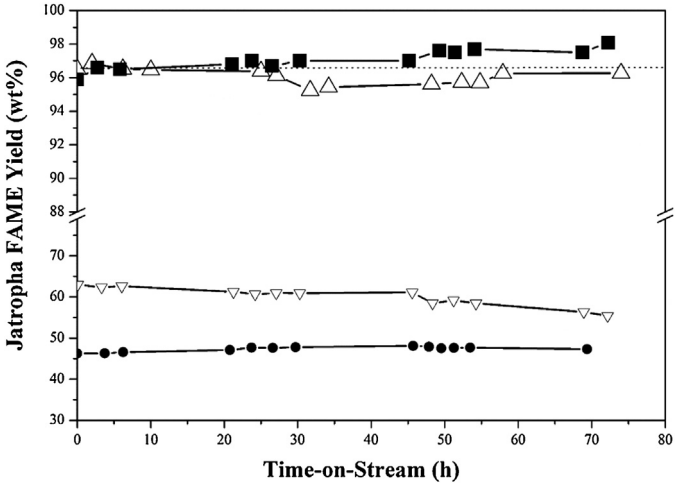

Fig. 10. Production of Jatropha BDFs as a function of time-on-stream over (■) N500-3Ti-SBA-15, (△) A500-3Ti-SBA-15, (▽) extruded TiO_2 and (●) TS-1 materials at 180 °C and 5 bar, where the WHSV of Jatropha oil and the methanol-to-oil molar ratio are kept at 0.50 h^{-1} and 100, respectively.

channeling pores, which speed molecular diffusion and reduce possibility of pore blockage, give high Jatropha BDF yields in continuous fixed-bed reaction system even if the time-on-stream is longer than 70 h. By contrast, the commercial TS-1 and extruded TiO_2 give low Jatropha BDF yields at the same reaction condition, due to low molecular diffusion through the microporous or randomly-distributed pores. Noted that that the Jatropha BDF yield over the A500-3Ti-SBA-15 material is slightly varied as the time-on-stream is prolonged. It implies that the porous silica framework is probably unstable or blocked after a long reaction period. To clarify the deactivation mechanism, the used A500-3Ti-SBA-15 and N500-3Ti-SBA-15 catalysts were simply washed with acetone, dried at 50 °C and then characterized by N_2 physisorption, pore size analysis and thermal analysis. The N_2 physisorption data show that the S_{BET} and V_{Total} values of used A500-3Ti-SBA-15 and N500-3Ti-SBA-15 catalysts are significantly dropped and the Φ values are decreased from 7.2–7.3 nm to 5.6–6.0 nm, due to that large amounts of oil molecules are still remained in the pores (ESI, Figs. 6 and 7). Our previous studies have demonstrated that the oil molecules can be nearly removed from the used catalysts by solvent extraction or calcination [12,13,31,44–46]. After the regeneration by calcination in air or N_2, the porosity and pore ordering of the regenerated A500-3Ti-SBA-15 and N500-3Ti-SBA-15 materials are recovered, similar to those of the fresh counterpart materials (ESI, Fig. 6). Therefore, the pore blockage can be completely ruled out as a possible reason for deactivation of the A500-3Ti-SBA-15 material in continuous production of Jatropha BDF.

The composition and impurity of various Jatropha BDFs synthesized by the above catalysts were carefully analyzed by the GC and ICP-OES techniques (Table 3). The Jatropha BDF synthesized by the N500-3Ti-SBA-15 material contains ultra-high FAME content (96.9–98.2 wt%) with little amounts of soap building elements, phospholipids and undesired contaminations. The silica species leached from the N500-3Ti-SBA-15 material to Jatropha BDF are only 1.6–3.5 ppm, progressively decreased in increasing the reaction period. These data represent that the Jatropha BDF synthesized by the N500-3Ti-SBA-15 material can fulfill with the specification of the EN14214:2012 standard. By contrast, the Jatropha BDF synthesized by the A500-3Ti-SBA-15 material contains a considerable amount of Si species in the range of 88–133 ppm although the FAME content is pretty high. The regenerated A500-3Ti-SBA-15 material shows lower surface area and porosity than the regenerated N500-3Ti-SBA-15 material (ESI, Fig. 6). It is clear that the deactivation of

the A500-3Ti-SBA-15 material is mainly caused by serious leaching of mesoporous silica framework in the integrated process for BDF production. Besides, it should be noticed that the unreactive impurities, such as TG, DG and MG, of Jatropha BDF synthesized by the A500-3Ti-SBA-15 material are all higher than the specification of the EN14214:2012 standard. The commercial TS-1 zeolite and extruded TiO_2 nanoparticles could hardly be worse suited for production of high-quality Jatropha BDF. The post-treatment units, such as washing, separation and purification, are necessary before the Jatropha BDFs synthesized by commercial TS-1, extruded TiO_2 and A500-3Ti-SBA-15 materials are blended with petro–diesel for car use. Based on the catalytic studies through batch-type and fixed-bed reaction systems, it can be said that the carbonaceous 3Ti-SBA-15 material as a highly efficient and durable solid acid catalyst is suitable for production of high-quality Jatropha BDF on a large scale, which can be blended with petro-diesel without further post-treatment.

4. Conclusions

Carbonaceous Ti-SBA-15 materials with enhanced activity and durability had been successfully synthesized by the self-assembly process and carbonization, and applied as Lewis solid acid catalysts for transesterification of Jatropha oil with methanol into high-quality Jatropha BDF in both batch-type and fixed-bed reaction systems. Thorough characterizations confirmed that the catalytically active sites were related to the tetrahedrally coordinated Ti species with weakly Lewis acid property, which could be maximized in the superficial areas when the HCl/TTIP molar ratio in the Ti precursor was kept at 2.5. The leaching of silica was minimized by covering the mesoporous silica framework with a light coating of carbon species derived from direct carbonization of the P123 templates as the only carbon source originally inside the channeling pores. The carbonization process described in this study was low cost and environmental friendly, where neither sulfuric acid nor sugar was added. The carbonaceous Ti-SBA-15 materials with maximum Ti sites in the tetrahedral coordination spheres and largely channeling pores exhibited excellent activity and durability in production of high-quality Jatropha BDF in both batch-type and fixed-bed reaction systems, as compared with commercial TS-1 zeolite, powdered and extruded TiO_2 nanoparticles and counterpart materials with bare silica framework. It is therefore believed that the carbonaceous Ti-SBA-15 materials show promise as highly active and durable solid acid catalysts for production of high-quality Jatropha BDF on an industrial scale, which fulfills with the specification of the international fuel standard.

Acknowledgements

This research was supported by JST-JICA's SATREPS project. Acknowledgements are extended to Dr. A. Endo and Dr. A. Kawai of Research Institute for Chemical Process Technology, AIST, for XRD experiment, Dr. Y. Miseki and Dr. K. Sayama of Research Center for Photovoltaics (RCPV), AIST, for UV–vis experiment, and Mr. M. Kaitsuka and Dr. M. Oguma of Research Institute for Energy Conversion, AIST, for ICP-OES analysis.

Appendix A. Supplementary data

Supplementary data associated with this article can be found, in the online version, at http://dx.doi.org/10.1016/j.apcatb.2015.08.053.

References

[1] I. Mukherjee, B.K. Sovacool, Renew. Sustain. Energy Rev. 37 (2014) 1–12.
[2] M.D. Serio, R. Tesser, L. Pengmei, E. Santacesaria, Energy Fuel 22 (2008) 207.
[3] H.J. Berchmans, S. Hirata, Bioresour. Technol. 99 (2008) 1716.
[4] I.J. Stojkovic, O.S. Stamenkovic, D.S. Povrenvic, V.B. Veljkovic, Renew. Sustain. Energy Rev. 32 (2014) 1–15.
[5] V.B. Veljkovic, O.S. Stamenkovic, M.B. Tasic, Renew. Sustain. Energy Rev. 32 (2014) 40–60.
[6] J.A. Melero, J. Iglesias, G. Morales, Green Chem. 11 (2009) 1285.
[7] K. Wilson, A.F. Lee, Catal. Sci. Technol. 2 (2012) 884.
[8] A.F. Lee, J.A. Bennett, J.C. Manayil, K. Wilson, Chem. Soc. Rev. 43 (2014) 7887.
[9] T. Oku, M. Nonoguchi, T. Moriguchi, PCT. Patent 2005/021697 A1 (2005).
[10] M. Cozzolino, R. Tesser, M. Di Serio, M. Ledda, G. Minutillo, E. Santacesaria, Stud. Surf. Sci. Catal. 162 (2006) 299.
[11] M. Cozzolino, M. Di Serio, R. Tesser, E. Santacesaria, Appl. Catal. A: Gen. 325 (2007) 256.
[12] S.Y. Chen, T. Mochizuki, Y. Abe, M. Toba, Y. Yoshimura, Catal. Commun. 41 (2013) 136.
[13] S.Y. Chen, T. Mochizuki, Y. Abe, M. Toba, Y. Yoshimura, Appl. Catal. B: Environ. 148–149 (2014) 344.
[14] W.W. Lukens, P. Schmidt-Winkel, D.Y. Zhao, J. Feng, G.D. Stucky, Langmuir 15 (1999) 5403.
[15] W.W. Lukens, P. Yang, G.D. Stucky, Chem. Mater. 13 (2001) 28.
[16] S.Y. Chen, Y.T. Chen, J.J. Lee, S. Cheng, J. Mater. Chem. 21 (2011) 5693.
[17] D. Zhao, J. Feng, Q. Huo, N. Melosh, G.H. Fredrickson, B.F. Chmelka, G.D. Stucky, Science 279 (1998) 548.
[18] S.Y. Chen, C.Y. Tang, W.T. Chuang, J.J. Lee, Y.L. Tsai, J.C.C. Chan, C.Y. Lin, Y.C. Liu, S. Cheng, Chem. Mater. 20 (2008) 3906.
[19] Y. Chen, Y. Huang, J. Xiu, X. Han, X. Bao, Appl. Catal. A: Gen. 273 (2004) 185.
[20] F.T. Kuo, S.Y. Chen, T.H. Lin, J.F. Lee, S. Cheng, RSC Adv. 3 (2013) 12604.
[21] C.H. Chen, C.H. Liua, Y.C. Su, C.M. Yang, Appl. Catal. B: Environ. 123–124 (2012) 36.
[22] R. Ganguly, V.K. Aswal, P.A. Hassan, I.K. Gopalakrishnan, J.V. Yakhmi, J. Phys. Chem. B 109 (2005) 5653.
[23] P. Linton, J.C. Hernandez-Garrido, P.A. Midgley, H. Wennerström, V. Alfredsson, Phys. Chem. Chem. Phys. 11 (2009) 10973.
[24] P. Linton, H. Wennerström, V. Alfredsson, Phys. Chem. Chem. Phys. 12 (2010) 3852.
[25] N. Reichhardt, T. Kjellman, M. Sakeye, F. Paulsen, J.H. Smatt, M. Linden, V. Alfredsson, Chem. Mater. 23 (2011) 3400.
[26] A. Thangaraj, R. Kumar, P. Ratnasamy, J. Catal. 131 (1991) 294.
[27] P. Wu, T. Tatsumi, T. Komatsu, T. Yashima, J. Catal. 202 (2001) 245.
[28] S.Y. Chen, C.Y. Tang, J.F. Lee, L.Y. Jang, T. Tatsumi, S. Cheng, J. Mater. Chem. 21 (2011) 2255.
[29] M.S. Wong, H.C. Huang, J.Y. Ying, Chem. Mater. 14 (2002) 1961.
[30] S.Y. Chen, J.F. Lee, S. Cheng, J. Catal. 270 (2010) 196.
[31] S.Y. Chen, S. Lao-ubol, T. Mochizuki, Y. Abe, M. Toba, Y. Yoshimura, Appl. Catal. A: Gen. 485 (2014) 28.
[32] M. Kruk, M. Jaroniec, C.H. Ko, R. Ryoo, Chem. Mater. 12 (2000) 1961.
[33] P.I. Ravikovitch, A.V. Neimark, J. Phys. Chem. B 105 (2001) 6817.
[34] C.M. Yang, B. Zibrowius, W. Schmidt, F. Schuth, Chem. Mater. 16 (2004) 2918.
[35] P. Yang, D. Zhao, D.I. Margolese, B.F. Chmelka, G.D. Stucky, Nature 396 (1998) 152.
[36] M. Bowman, D. Hilligoss, S. Rasmussen, R. Thomas, Hydrocarbon Process 85 (2006) 103.
[37] X. Yan, H. Song, X. Chen, J. Mater. Chem. 19 (2009) 4491.
[38] L. Li, H. Song, X. Chen, Microporous Mesoporous Mater. 94 (2006) 9.
[39] X. Yan, H. Song, X. Chen, J. Mater. Chem. 19 (2009) 4491.
[40] P. Valle-Vigon, M. Sevilla, A.B. Fuertes, Microporous Mesoporous Mater. 134 (2010) 165.
[41] H.N. Pham, A.E. Anderson, R.L. Johnson, K. Schmidt-Rohr, A.K. Datye, Angew. Chem. Int. Ed. 51 (2012) 13163.
[42] S. Inagaki, S. Guan, T. Ohsamu, O. Terasaki, Nature 416 (2002) 304.
[43] A.B. Fuertes, T.A. Centeno, J. Mater. Chem. 15 (2005) 1079.
[44] F.T. Kuo, S.Y. Chen, T.H. Lin, J.F. Lee, S. Cheng, RSC Adv. 3 (2013) 12604.
[45] S.Y. Chen, T. Yokoi, C.-Y. Tang, L.-Y. Jang, T. Tatsumi, J.C.C. Chan, S. Cheng, Green Chem. 13 (2011) 2920.
[46] S.Y. Chen, S. Lao-ubol, T. Mochizuki, Y. Abe, M. Toba, Y. Yoshimura, Bioresour. Technol. 157 (2014) 346.